Exciton pattern generation in GaAs/$Al_xGa_{1-x}As$ multiple quantum wells

B. Fluegel, K. Alberi, L. Bhusal, and A. Mascarenhas
National Renewable Energy Laboratory, 1617 Cole Boulevard, Golden, Colorado 80401, USA

D. W. Snoke
Department of Physics and Astronomy, University of Pittsburgh, Pittsburgh, Pennsylvania 15260, USA

G. Karunasiri
Department of Physics, Naval Postgraduate School, Monterey, California 93943, USA

L. N. Pfeiffer and K. West
Bell Laboratories, Lucent Technologies, Murray Hill, New Jersey 07974, USA
(Received 23 December 2010; published 16 May 2011)

Exciton photoluminescence pattern generation is investigated in multiple quantum wells. High-contrast outer rings and localized bright spots are generated using efficient field-assisted upconversion of laser light whose photon energy lies below the energy of the luminescing quantum well transition. Time-resolved images of the bright spots reveal unexpected dynamics that are not explained by two-dimensional rate equations for generation and diffusion. This behavior can be understood as a result of three-dimensional transport in the vertically extended samples.

DOI: 10.1103/PhysRevB.83.195320 PACS number(s): 78.67.De, 78.55.Cr, 71.35.−y

I. INTRODUCTION

Recently, fabrication techniques of GaAs and InGaAs quantum wells have reduced the various disorder contributions to the point where photogenerated charge carriers can diffuse in the plane of the well for hundreds of microns, enabling the study of very cold carrier populations far from the excitation spot. A striking demonstration of this was the publication[1,2] of exciton photoluminescence (PL) ring images in double quantum wells (DQW) under an electric field. In spatially resolved measurements, the PL of the indirect exciton of the DQW was seen at the laser excitation spot, and also in a sharp ring-shaped region surrounding it, with large regions of dark sample separating the two. Similar rings were also observed centered at "localized bright spots" (LBS), the name given to fixed point locations on the sample, remote from the laser, that emit strong PL.[3,4] These results are important examples of the ability to increase the lifetime of photogenerated direct-gap semiconductor charge carriers to microseconds through vertical and lateral charge separation.[5,6] Quantum transport measurements of high-mobility two-dimensional electron gases, for example, are usually performed in doped electron populations, since direct-gap semiconductor lifetimes do not permit photogenerated electrons to fully cool to the lattice temperature. With inhibited recombination, an ultracold electron population could be photogenerated, allowing dynamical spatial and temporal control via the exciting laser.

A crucial element in the exciton pattern formation was found to be[3,7,8] the recombination of an electrically injected carrier species with an optically injected, oppositely charged one. In the case of the outer ring identified in Ref. 1, the external electrical bias injects a spatially broad electron density drifting from the contacts of the *n-i-n* structure. Its density under no illumination affects how far the spatially focused photohole population can deplete electrons, thus determining the ring diameter. Note that the optically injected electrons rapidly tunnel out of the well due to lower effective mass, leaving a large hole population at the laser spot which diffuses laterally.[3,8] The ring is formed at a diameter from the laser where the densities of the electrically injected electron population and the diffusing hole populations are nearly the same. A lower electron density yields a weaker but larger diameter ring. In the *n-i-n* structures used in Refs. 1 and 2 the minimum electron density was limited by the amount of modulation doping from the contacts. In the present study we have placed the 2DEG in the depletion region of a reverse-biased *p-i-n* junction, allowing the injected electron density from leakage current to be varied over a wider range. Also, because the spatially indirect exciton of the DQW is not a strict requirement for ring formation,[7,8] we have instead used multiple (uncoupled) quantum wells (MQW) for a greater interaction length. We find that long-range lateral transport can occur with electron and hole creation in bulk GaAs, below the MQW's lowest confined energies, followed by field-induced tunneling into the MQW. The result is an unusually efficient upconversion PL ring, emitting at an energy higher than the excitation laser. Rings are also observed at fixed points outside the excitation spot and the temporal evolution of these remote rings reveals that they are driven by carriers transported from the laser spot.

II. EXPERIMENT

Our sample, similar to that in Ref. 5 and shown schematically in Fig. 1, contains 20 periods of GaAs/AlGaAs multiple quantum wells (MQW) symmetrically positioned between 500 Å AlGaAs barriers and 1000 Å GaAs spacers. Additionally, an 80 Å DQW is placed at the center of the MQW allowing the internal electric field to be monitored through the energy of the indirect exciton. Its 500 Å AlGaAs outer barriers affect device current, but the DQW itself does not contribute

1098-0121/2011/83(19)/195320(6) ©2011 American Physical Society

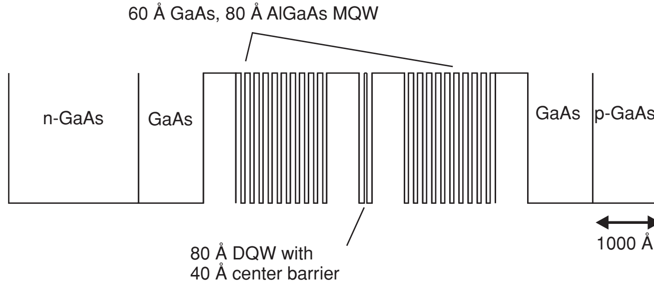

FIG. 1. Schematic of the sample structure showing the conduction band height and the layer thicknesses drawn to scale. The n-GaAs is the first layer grown on an n^+ substrate. $Al_{0.3}Ga_{0.7}As$ is used for the barriers. Total thickness of the intrinsic region is 0.70 μm.

to the results presented. This structure comprises the intrinsic region of a p-i-n diode. A similar diode, but without the DQW, was also studied for comparison. Values of the bias reported here are the total of the voltage applied to the top p contact and a built-in potential of −1.5 V estimated from the Stark shift of the DQW indirect exciton. PL and photocurrent (PC) measurements were made at low temperature using cw and mode-locked lasers. PL was detected with an uncooled charge-coupled device (CCD) camera and Raman edge interference filters for images, with a spectrometer and cooled CCD for spectra, and with a spectrometer and streak camera for time-resolved data.

III. RESULTS

Figure 2(a) shows the PL image obtained under 1.96 eV illumination and −4.5 V bias. The image is filtered at 1.60 eV to select the energy of the lowest confined heavy-hole to electron transition in the MQW [1.594 eV in Fig. 7(a)] and a weak ring is seen similar to that in Ref. 8. This excitation energy is above the thick AlGaAs barrier's band gap, a condition which was found in Ref. 7 to be a necessary requirement for ring formation in single quantum wells and DQWs. However, a study of the excitation energy dependence of the present structure reveals that the effect does not require photon energy above the barrier height, and in fact, the highest contrast ring structures were obtained using a laser tuned *below* 1.594 eV. Figure 2(b) shows a ring generated by this upconversion photoluminescence (UPL) within the MQW.

To determine the physical mechanism by which the 1.53 eV laser generates UPL from the MQW at 1.6 eV, we have measured the upconversion photoluminescence excitation (UPLE) spectra for different bias voltages as shown in Fig. 3. In the UPLE technique, scanning the excitation laser energy will maximize the upconversion signal when the laser energy coincides with optically allowed transitions of the absorbing layers; these energies can identify the absorbing layers in a multistep excitation process. In Ref. 9, for example, also in a GaAs/AlGaAs structure, sharp peaks in the UPLE spectrum clearly identified the wide quantum well absorption that occurred in a two-step, two-photon process giving particularly strong upconversion. For the present sample, the −3.5 V UPLE spectrum in Fig. 3 shows a ~25-meV-wide onset at 1.525 eV and a very small peak/dip at the DQW direct exciton energy (1.575 eV). For any laser photon energy, the UPL signal

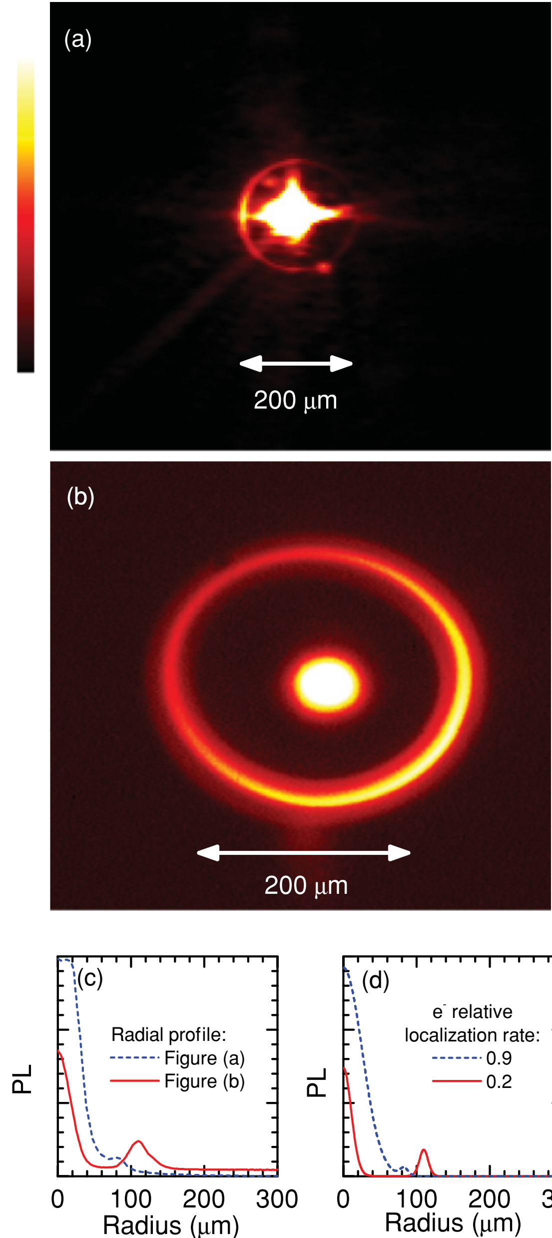

FIG. 2. (Color online) Comparison of a MQW PL ring through direct excitation at 1.96 eV (a) and through upconversion exciting at 1.53 eV (b). The cw laser powers are 0.6 mW and 1 mW, respectively, and the bias is −4.5 V. (c) Radial profiles of the images in (a) (dashed line) and (b) (solid line). (d) Numerical calculation of the ring profile for two different electron localization rates: 0.9 × the hole rate (dashed line) and 0.2 × the hole rate (solid line).

vanishes at zero applied bias and rises monotonically with strength of the electric field. The latter is shown in detail in the inset of Fig. 3, where the spectrally integrated UPL peak is plotted in a log plot as a function of the inverse bias voltage.

The external bias source supplies energy to the upconversion process in the form of PC which is plotted in Fig. 4 next to a UPLE spectrum taken concurrently. In the upconversion regime, where $\hbar\omega_{laser} < 1.60$ eV, both curves have the same spectral features: a broad threshold at 1.500 eV

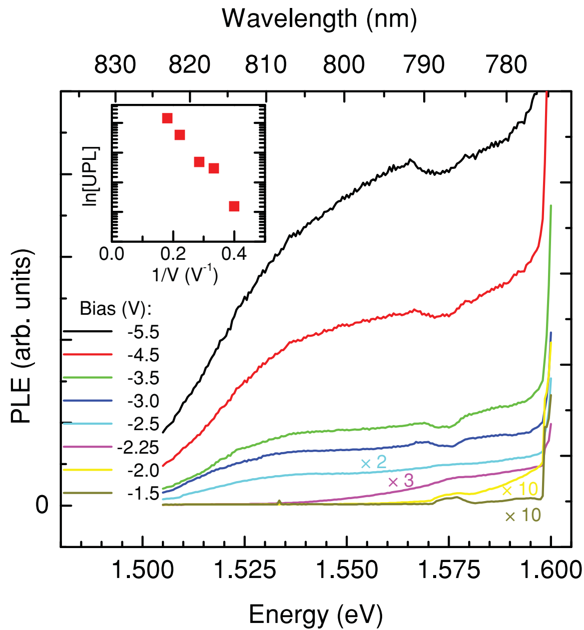

FIG. 3. (Color online) UPLE measurements showing the upconverted MQW PL at 1.60 eV as a function of laser photon energy, for bias voltages ranging from −5.5 V (upmost curve) to −1.5 V (lowest curve). Lower curves are scaled by the factors shown. The cw laser power was held at 63 μW and the sample at 1.7 K. Inset: log plot of the magnitude of the spectrally integrated MQW PL peak as a function of the inverse bias voltage, with the laser tuned to 1.55 eV.

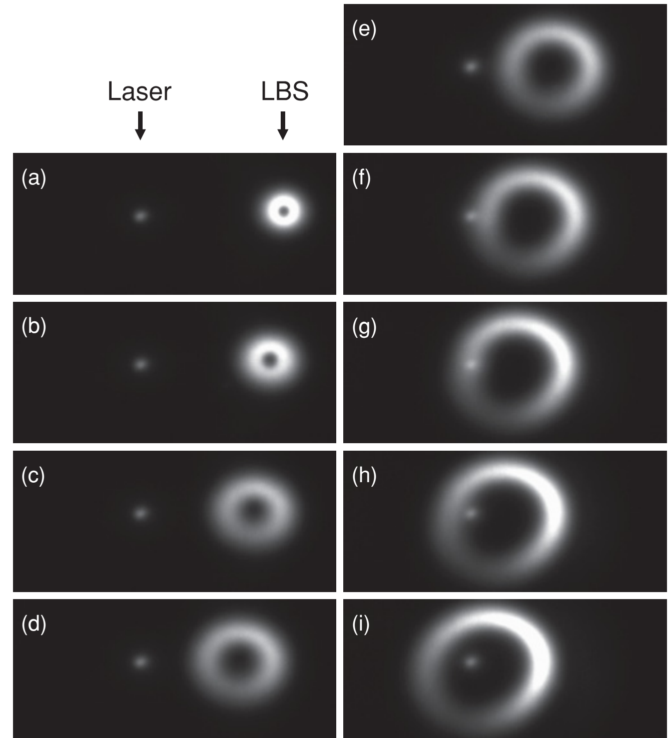

FIG. 5. Sequence of spatial PL maps taken as the sample is moved to bring the LBS (moving ring) closer to the point of laser excitation (fixed point of weaker PL). The separation between the two is 70 μm in frame (a). The sample is held at 9 K, −4.0 V bias and the cw excitation is 80 μW at 792 nm focused to 1 μm.

to 1.525 eV, and broad peak at 1.530 eV, followed by a flat continuum.

Using the measurement conditions of Fig. 2(b), we also find LBS, particularly in sample regions where the laser-centered ring is weak or undetectable. Within a limited range of laser power, rings are observed around the LBS as shown in Fig. 5. The sequence of frames in Fig. 5 shows the ring's progression as the LBS is physically moved closer to the laser point. As discussed below, this behavior is not consistent with the model of Ref. 3, and to explore this fully, we have used streak camera measurements to reveal the creation and decay of an LBS ring, presented in Fig. 6. As in Fig. 5, the frames show the effect of decreasing the laser-to-LBS distance. The intense streak in the upper left of Fig. 6(a) is the excitation spot where the upconversion PL temporally follows the 30 ns laser pulse. The LBS is 300 μm from that point. Approximately 80 ns after the leading edge of the laser pulse, a ring begins expanding about the LBS reaching a diameter of 16 μm after $t = 130$ ns. That diameter increases as the sample is translated to bring the LBS closer to the laser spot in Figs. 6(b)–6(h), in agreement with Fig. 5. The initial transient occurs at an increasingly earlier time through Figs. 6(b)–6(h).

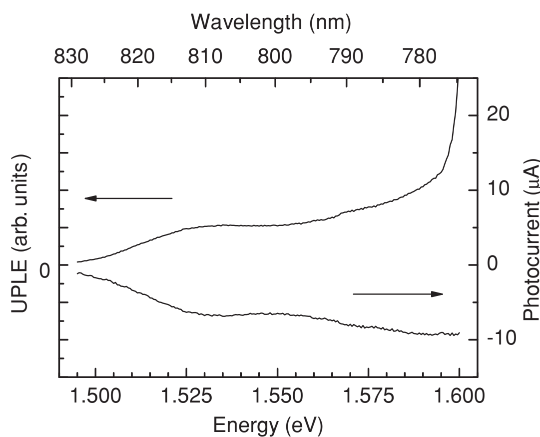

FIG. 4. Comparison of photocurrent and UPLE spectra measured at 80 K using a cw laser power of 160 μW.

IV. DISCUSSION

The mechanism of the PL upconversion can be understood from analysis of Fig. 3. The photoabsorbing layer is identified by noting that the broad excitation edge in the UPLE spectra at 1.525 eV is close to the band gap of the undoped GaAs spacer layers. The large width of this edge can be attributed to the electric field. Sharp excitonic PL at 1.51 eV from these layers was observed at zero bias, but it quenched at only a few × 0.1 V of reverse bias. This is consistent with an electric field ionization of the excitonic enhancement[10] in GaAs, resulting in a broad absorption edge and UPLE threshold. After photogeneration, electrons and holes must gain energy in transferring from the GaAs to the MQW. Similar efficient upconversion has been previously observed in resonant tunneling structures[11] in which an electric field

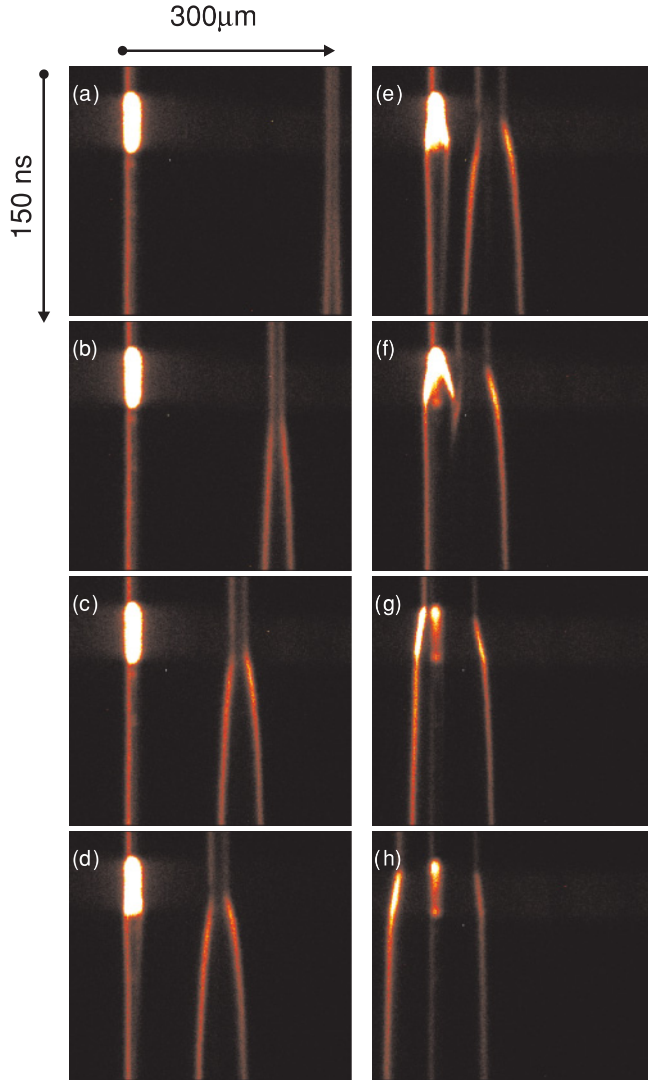

FIG. 6. (Color online) Sequence of spatial-temporal streak camera sweeps taken as the sample is moved to bring the LBS closer to the point of laser excitation. A horizontal slice of the spatial map has been imaged on the streak camera input slit and temporally dispersed in the vertical direction. The sample is at 10 K and −3.1 V bias. A 795 nm laser was gated on for 30 ns at 200 kHz with a pulse energy of 100 pJ. Weak signals outside this time window at the excitation spot, and for prior times near the LBS spot, are an artifact due to cw leakage of the laser gate.

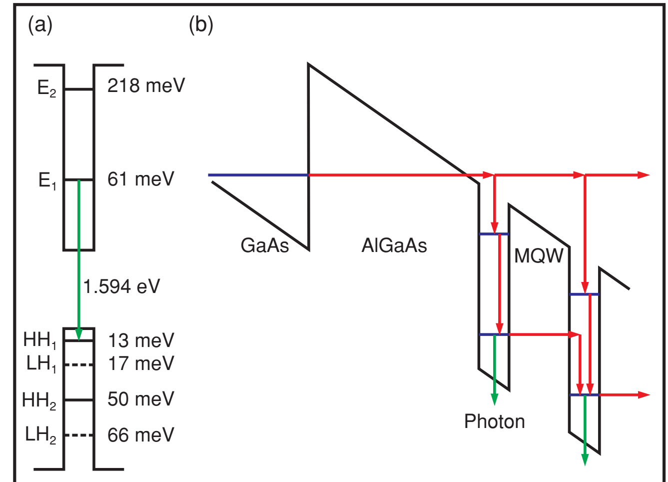

FIG. 7. (Color online) (a) Calculated electron, heavy-hole, and light-hole confinement energies for the MQW. (b) Schematic diagram of the conduction band as a function of growth direction, showing one GaAs spacer, an AlGaAs barrier, and part of the MQW. The band bending under an electric field causes tunneling (horizontal arrows) of carriers photogenerated in the GaAs, through the barrier and into the MQW.

provided the energy to transfer electrons and holes from a lower band gap layer into a single quantum well. This scheme is demonstrated in Fig. 7(a), which shows the calculated electron, light-hole, and heavy-hole bound-state energies in the MQW using a transfer matrix approach. The bending of bands due to the bias (internal + applied) is shown in Fig. 7(b), where the tunneling electrons from the GaAs contact layer get trapped in the MQW. Electrons that drop down to the ground state will recombine with holes that have similarly tunneled from the lower GaAs buffer layer to produce high-energy photons. In a simple approximation for large barrier heights,[12] the tunneling rate R for electrons of effective mass m^* through a potential barrier V_0 in an electric field E is found by the WKB approximation to the Schrödinger equation for a triangular potential, yielding

$$R = R_0 \exp\left(-\frac{4\sqrt{2m^*}}{3\hbar}\frac{V_0^{3/2}}{eE}\right). \tag{1}$$

The functional form of this can be compared to the inset of Fig. 3. With the laser fixed at 1.55 eV, and for the smallest values of reverse bias, the measured magnitude of the integrated UPL is complicated by a vanishing energy gain (see main figure and discussion below). However, for reverse bias $\geqslant$2.5 V, as seen in the inset, the dependence is nearly exponential, agreeing with Eq. (1).

The upconversion generation of the MQW PL is far more efficient than bulk semiconductor two-photon absorption in the absence of a field. It is approximately 1% of that obtained by direct resonant excitation at 1.60 eV, and by using a higher reverse bias of 8.5 V this relative efficiency can be optimized to 27%. The energy gain available for this upconversion (output photon energy − input photon energy) is proportional to the potential drop across the 500 Å AlGaAs barrier, and for bias voltage $V \geqslant -2.25$ V, upconversion is only possible at a reduced gain, as seen in the lower curves of Fig. 3. Conversely, for the smaller bias voltage used in the upper curves, the available energy gain exceeds the MQW confinement energies ($E_1 + \mathrm{HH}_1$), and thus even higher gain upconversion devices might be designed by decreasing the well width.

For steady-state UPL to occur, the MQW must be located between GaAs spacer layers, so that photogenerated holes are supplied by a complementary absorption and tunneling process from the GaAs layer on the n-doped, substrate side [lower part of Fig. 8(a)]. The emission of a single upconverted photon therefore should require two laser photons, one absorbed in each GaAs spacer. Of the two resulting electron-hole pairs, the higher potential electron and hole tunnel into the MQW and generate the UPL while the lower potential electron and

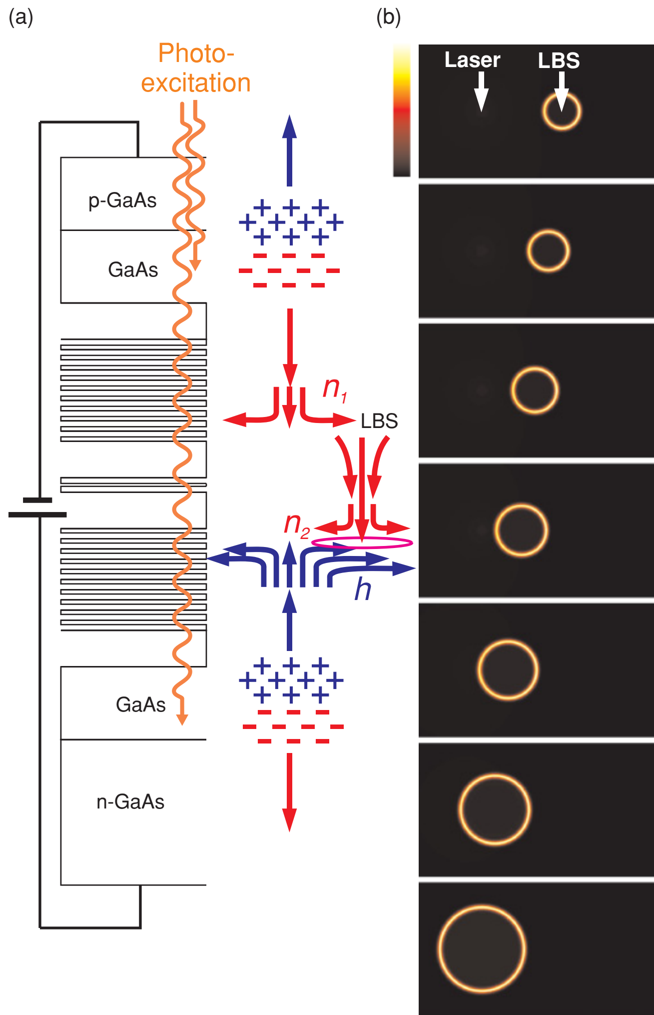

FIG. 8. (Color online) (a) Schematic of charge transport near LBS. Left side shows GaAs and AlGaAs layers distinguished by their conduction band height. See Fig. 1 for identification of individual layers. The laser is absorbed in the thick GaAs layers. Right side shows the generation of the electron and hole populations that drift and tunnel (vertical arrows) and laterally diffuse (90° arrows). LBS marks an isolated location where electrons are funneled through a breakdown in the DQW AlGaAs barriers. Exciton ring generation occurs at points where diffused holes meet expanding electrons. n_1, n_2, and h are the three carrier populations modeled by rate equations. (b) Calculated photoluminescence intensity ($n_2 \times h$) maps for the steady-state solution of the model diagrammed in (a). From upper to lower image, the LBS separation from the laser is 600 μm, 500 μm, 400 μm, 300 μm, 200 μm, 100 μm, and 0. The laser excitation and the LBS tunneling probability have Gaussian profiles with full width at half maximum of 60 μm and 20 μm.

hole are swept out to the external circuit. This is confirmed by the similarity of UPLE and PC in Fig. 4. The energy gain (UPLE) and energy loss (PC) have similar spectral dependence because they are both simultaneous results of the same absorption process. Further support comes from the small dip of the UPLE at 1.575 eV in the upper curves of Fig. 3. This is the energy of the DQW's direct exciton and thus the energy of its absorption edge since the direct exciton is the lowest energy spatially direct transition. The 1.575 eV dip in signal is due to attenuation of the laser as it passes through the DQW, proving that laser absorption in the layers beneath the DQW also contributes to the upconversion process.

From the results of Figs. 3 and 4, we conclude that field-driven upconversion similar to that in Ref. 11 is capable of exciting hot carriers into the MQW. Ring formation then occurs from diffusion dynamics similarly to that in Refs. 3 and 8. The strong image contrast, i.e., the intensity ratio between the ring and excitation spot that is seen in Fig. 2(b), can be understood from numerical calculation of the rate equations of Ref. 8. In Ref. 8 that contrast depends strongly on the degree to which holes are photoexcited and preferentially (compared to electrons) localized into the wells. This is demonstrated by the calculated profiles shown in Fig. 2(d), which are a fit of the rate equations' excitation parameters to the measured profiles of the UPL ring and the direct-excitation ring in Fig. 2(c). The higher ring contrast measured with UPL is reproduced in the model by using a greater inequality in the electron and hole generation rates, which for the present sample we attribute to unequal tunneling rates.

Unlike the laser-centered rings, the LBS rings in Fig. 5 cannot be explained by comparison with previous works. In Ref. 3 these were observed within a large sample area uniformly illuminated by a defocused laser. They were explained as points of electrical leakage of electrons within a large region of photogenerated holes, giving a carrier density profile that is reversed from what happens around a focused laser spot. Increasing the laser power decreased the ring diameter. Calculations[3] reproduced the ring shape and the observed inverted laser power dependence, with the necessary restriction that the LBS can only be observed inside the diameter of the laser-centered ring. The LBS rings in the present work cannot be explained by this simple model. They occur using a focused laser, and can be observed at large distances from the laser in sample regions that do not show a laser-centered ring, as shown in Fig. 5(a). By interpreting this figure as a region of vanishing electron density, the LBS ring might still be understood as a point of electron injection. However, this would fail to explain the full spatial dependence of Fig. 5, where it is seen that the ring centered at the LBS *increases* in diameter as it is moved closer to the laser. In the model of Ref. 3, the LBS radius must shrink as the LBS is moved into higher hole density, which would be expected near the laser. This would make a pattern such as Fig. 5(h) impossible. Complications to this steady-state argument may arise if the approaching LBS modifies the absorption or tunneling at the laser point. For this reason we consider additionally the time-resolved LBS ring of Fig. 6. For each value of laser-to-LBS separation, the time delay between the laser pulse and the onset of ring expansion is proportional to the spatial separation, indicating that the ring is caused by at least one carrier population that originates and expands from the laser spot. Furthermore, the nature of the initial ring dynamics at any fixed distance, i.e., a symmetrical and temporally growing diameter, is again in opposition to the inverted electron-hole contrast of Ref. 3. This last observation is independent of possible complications from the unknown effects of moving the LBS location. It indicates that the carrier population expanding from the LBS is laser driven, not current driven.

In order to understand how photogenerated carriers can diffuse from the laser and radiate again from a point that is 300 μm distant, we note that in numerically modeling the ring formation, the general requirements are a diffusing point source of one carrier species located within a spatially extended cloud of the other carrier species. The ultimate origin of our LBS might be very similar to that of Ref. 3: a point of weaker potential in the thick barriers surrounding the DQW. Rather than being a point source of electrical injection as in the *n-i-n* model, this spot in our *p-i-n* device serves as an accelerated tunneling point for the laterally diffusing photogenerated electrons that accumulate in front of the barrier. The LBS is then a point electron source into the lower MQW. The upper part of Fig. 8(a) shows this schematically. The photogenerated holes drifting up from the lower GaAs layer also diffuse in front of the DQW outer barriers. Their lateral extent is greater than the electrons due to a slower tunneling rate.

The schematic model of Fig. 8(a) can be approximated by a set of three rate equations for n_1, n_2, and h, which are respectively the electron density in the upper MQW and the electron and hole densities in the lower MQW. Diffusion is included and source terms generate n_1 at the laser focus and h at all points. Tunneling is modeled by decay from n_1 to n_2 with a weak term that is spatially uniform and a stronger term localized at the LBS point. As in Refs. 3 and 8, photoluminescence from the recombination of n_2 and h is included as a decay of both densities that is proportional to their product. Figure 8(b) shows intensity plots of the PL obtained by numerical steady-state solutions of the three rate equations for several separation distances of the laser and LBS. A ring-shaped PL pattern is centered at the LBS where the n_2 electrons tunneling out of the LBS meet the spatially extended hole cloud. Moving the LBS closer to the laser results in a stronger tunneling current and hence a larger ring, agreeing with the observed results of Fig. 5. Relatively little PL occurs at the laser and LBS locations due to the strong diffusion.

In general, the result of vertical carrier drift allows for more complex exciton pattern generation such as Fig. 5(h) since electrons and holes can diffuse on different planes before meeting to radiatively recombine. The ability to actually direct the transport of photogenerated carriers to a specific point, beyond simple free diffusion and over hundreds of microns, opens direct-gap III–V materials to greater possibilities for electronic design. Indirect excitons have been used to demonstrate this type of transport in growth-induced[13] and stress-induced potential wells;[6] the results of Fig. 5 show that this can also be done with unbound carriers.

In conclusion, the exciton ring PL image originally seen in DQWs is also observed in a *p-i-n* MQW structure at PL energies higher than the laser. The upconversion, occurring at the central laser spot, results from a bipolar field-assisted tunneling through a symmetrical arrangement of layers. The excitation dynamics of the LBS ring diameter is contrary to simple 2D models and requires analysis of the full 3D nature of the carrier transport.

ACKNOWLEDGMENTS

Research at NREL was supported by the U.S. Department of Energy, Office of Basic Energy Sciences, Division of Materials Sciences and Engineering under Award DE-AC36-08GO28308.

[1] L. V. Butov, A. C. Gossard, and D. S. Chemla, Nature (London) **418**, 751 (2002).
[2] D. Snoke, S. Denev, Y. Liu, L. Pfeiffer, and K. West, Nature (London) **418**, 754 (2002).
[3] L. V. Butov, L. S. Levitov, A. V. Mintsev, B. D. Simons, A. C. Gossard, and D. S. Chemla, Phys. Rev. Lett. **92**, 117404 (2004).
[4] J. Butov, J. Phys. Condens. Matter **16**, R1577 (2004).
[5] Z. Vörös, R. Balili, D. W. Snoke, L. Pfeiffer, and K. West, Phys. Rev. Lett. **94**, 226401 (2005).
[6] Z. Vörös, D. W. Snoke, L. Pfeiffer, and K. West, Phys. Rev. Lett. **97**, 016803 (2006).
[7] D. Snoke, Y. Liu, S. Denev, L. Pfeiffer, and K. West, Solid State Commun. **127**, 187 (2003).
[8] R. Rapaport, Gang Chen, D. Snoke, Steven H. Simon, Loren Pfeiffer, Ken West, Y. Liu, and S. Denev, Phys. Rev. Lett. **92**, 117405 (2004).
[9] S. C. Hohng, D. W. Khang, Y. H. Ahn, J. Y. Lee, S. Y. Kihm, D. H. Kim, W. S. Kim, J. C. Woo, D. S. Kim, D. S. Citrin, D. H. Woo, E. K. Kim, S. H. Kim, and K. S. Lim, Phys. Rev. B **60**, 8883 (1999).
[10] D. Blossey, Phys. Rev. B **3**, 1382 (1971).
[11] M. S. Skolnick *et al.*, Phys. Rev. B **42**, 3069 (1990).
[12] See, e.g., S. Gasiorowicz, *Quantum Physics*, 3rd ed. (John Wiley & Sons, New York, 2003).
[13] L. V. Butov, C. W. Lai, A. L. Ivanov, A. C. Gossard, and D. S. Chemla, Nature (London) **417**, 47 (2002).